J. Fluid Mech. (2007), *vol.* 584, *pp.* 125–146.
doi:10.1017/S0022112007006465 Printed in the United Kingdom

Direct numerical simulation of the turbulent boundary layer over a rod-roughened wall

SEUNG-HYUN LEE AND HYUNG JIN SUNG†

Department of Mechanical Engineering, Korea Advanced Institute of Science and Technology, 373-1, Guseong-dong, Yuseong-gu, Daejeon, 305-701, Korea

(Received 16 June 2006 and in revised form 1 March 2007)

The effects of surface roughness on a spatially developing turbulent boundary layer (TBL) are investigated by performing direct numerical simulations of TBLs over rough and smooth walls. The Reynolds number based on the momentum thickness was varied in the range $Re_\theta = 300 \sim 1400$. The roughness elements were periodically arranged two-dimensional spanwise rods, and the roughness height was $k = 1.5\theta_{in}$, where θ_{in} is the momentum thickness at the inlet, which corresponds to $k/\delta = 0.045 \sim 0.125$, δ being the boundary layer thickness. To avoid generating a rough-wall inflow, which is prohibitively difficult, a step change from smooth to rough was placed $80\theta_{in}$ downstream from the inlet. The spatially developing characteristics of the rough-wall TBL were examined. Along the streamwise direction, the friction velocity approached a constant value, and self-preserving forms of the turbulent Reynolds stress tensors were obtained. Introduction of the roughness elements affected the turbulent stress not only in the roughness sublayer but also in the outer layer. Despite the roughness-induced increase of the turbulent Reynolds stress tensors in the outer layer, the roughness had only a relatively small effect on the anisotropic Reynolds stress tensor in the outer layer. Inspection of the triple products of the velocity fluctuations revealed that introducing the roughness elements onto the smooth wall had a marked effect on vertical turbulent transport across the whole TBL. By contrast, good surface similarity in the outer layer was obtained for the third-order moments of the velocity fluctuations.

1. Introduction

Turbulent boundary layers (TBLs) are observed in numerous fluid dynamic engineering applications, and many experimental and numerical studies have examined the characteristics of TBLs. In engineering applications involving wall-bounded boundary layer flow (e.g. automobiles, ships, airplanes and heat exchangers), the roughness of the wall surface is an important design parameter because it influences characteristics such as the transport of heat, mass and momentum. Although the effects of surface roughness on a TBL have been examined in many experimental and numerical studies, knowledge of these effects remains incomplete.

Previous studies on the effect of surface roughness on a TBL are reviewed well by Raupach, Antonia & Rajagopalan (1991) and Jimenez (2004). These reviews support the wall similarity hypothesis of Townsend (1976), which states that outside the roughness sublayer turbulent motions are independent of the surface roughness and

† Author to whom correspondence should be addressed: hjsung@kaist.ac.kr

that the interaction between the inner and outer layers is very weak at sufficiently large Reynolds numbers. They show that outside the roughness sublayer, both the defect form and the turbulent stresses normalized by a friction velocity are unaffected by roughening of the surface, consistent with Townsend's wall similarity hypothesis. In further support of this similarity hypothesis, Schultz & Flack (2003, 2005), Flack, Schultz & Shapiro (2005) and Connelly, Schultz & Flack (2006) recently observed that the outer layers of flows past smooth and rough walls were similar in terms of both mean flow and turbulent statistics. Jimenez (2004) proposed a criterion to satisfy the wall similarity: that the ratio between boundary layer thickness and roughness height (δ/k) should be larger than 40. Flack *et al.* (2005) and Schultz & Flack (2005) suggested that effective sand grain roughness height (k_s) is a better representative length scale than roughness height (k) for comparing the roughness effects of different roughness geometrical characteristics. They proposed an alternative criterion to satisfy the wall similarity with effective sand grain roughness height: that δ/k_s should be larger than 40, and the extent of the roughness sublayer is $5k_s$ rather than $5k$.

Results from several experimental studies have, however, been contrary to the wall similarity hypothesis. Krogstad, Antonia & Browne (1992) showed that the wake strength in a TBL is increased by surface roughness and that the interaction between the inner and outer layers is non-negligible. Krogstad & Antonia (1999) and Keirsbulck *et al.* (2002*a*) observed that turbulent Reynolds stresses in the outer layer of a TBL are significantly affected by the surface roughness. Smalley *et al.* (2002) found that a TBL on a rough wall exhibits lower anisotropy than that on a smooth wall. Bandyopadhyay & Watson (1988) and Antonia & Krogstad (2001) also observed that variations in the surface roughness significantly affect the high-order statistics in the outer layer. These experimental results oppose the notion that the outer layer of a TBL is insensitive to the surface roughness, and have led to considerable uncertainty regarding the effects of surface roughness on TBLs.

Recently, several numerical studies using DNS (direct numerical simulation) and LES (large-eddy simulation) have been conducted on turbulent channel flow with a rough wall. There are two basic types of rough-wall channel flow: flow through a symmetric channel in which upper and bottom walls are both roughened, and flow through an asymmetric channel that has one rough wall and one smooth wall. Lee (2002) performed a LES in a symmetric channel with three-dimensional roughness and found no significant difference between the turbulent stresses in the outer layers of the rough-walled channel and those of the corresponding smooth-walled channel. Ashrafian, Andersson & Manhart (2004) and Ashrafian & Andersson (2006*a*, *b*) performed a DNS of flow in a symmetric channel with either smooth walls or walls with a very small roughness ($k/h = 0.034$) achieved by placing two-dimensional rods on the walls. They found that the turbulent stresses, anisotropy, high-order statistics and Reynolds stress budgets in the outer layer were the same regardless of whether the walls were smooth or rough. Leonardi *et al.* (2003) performed a DNS of flow through an asymmetric channel with two-dimensional rod roughness and investigated the effect of varying the pitch between consecutive rods. They found that the turbulent stresses were considerably higher for the rough-walled channel than for the corresponding channel with smooth walls. However, they used a rod roughness of $k/h = 0.2$, which is too large to be considered as a surface roughness. Bhaganagar, Kim & Coleman (2004) performed a DNS of flow through an asymmetric channel with three-dimensional roughness and found that turbulent stresses in the outer layer were affected by surface roughness but vorticity fluctuations were relatively unaffected.

Krogstad *et al.* (2005) compared the experimental results of Bakken *et al.* (2005) for turbulent flow in a symmetric channel with a rod roughness of $k/h = 0.034$ with the results obtained by Ashrafian *et al.* (2004) from a DNS of the same height of rod roughness. They observed good agreement between the experimental and simulation results, with both showing no significant difference between the characteristics of the outer layer of the smooth wall and those of the rough wall. Note that these results are contrary to the behavior observed by Krogstad & Antonia (1999) in their rough-wall TBL experiments, which showed significant roughness effects in the outer layer. They conjectured that the degree to which surface roughness affects the outer layer is influenced by the flow type, for example symmetric channel flow, asymmetric channel flow, boundary layer, and so on.

Despite the fact that most experimental studies have examined the characteristics of TBLs, the majority of numerical studies (LES and DNS) have examined turbulent channel flows. This difference can be attributed to the difficulty of simulating TBLs. A TBL is a spatially developing flow, and hence periodic boundary conditions along the streamwise direction are not applicable. Moreover, realistic turbulent inflows must be generated at the inlet and the domain size along the downstream direction must be sufficiently large to accommodate the spatially developing flow. In particular, performing a DNS of a rough-wall TBL has two additional difficulties. First, to simulate a very small ratio of roughness height to boundary layer thickness, a finer grid spacing must be used along the streamwise and wall-normal directions, greatly increasing the computational expense. Second, because it is impossible to accurately generate a turbulent inflow characteristic of flow over a rough wall, DNS of flow over a rough wall must use a smooth-wall inflow, leading to a significant step change in the surface roughness from a smooth to a rough wall. To overcome this latter problem, the streamwise domain size must be sufficiently long for the flow to reach a new rough-wall equilibrium state after the roughness step change. These difficulties mean that DNS is computationally very expensive and complex. For these reasons, no DNS of a rough-wall TBL have been performed, and the absence of DNS data has made it difficult to validate experiments on rough-wall TBLs.

In the present study, we carried out DNS of TBLs with rough and smooth walls and compared our findings with previous experimental data. The objective was to elucidate the interaction between the inner and outer layers arising from the roughness and to delineate the basic characteristics of a rough-wall TBL. The Reynolds number was varied in the range $Re_\theta = 300 \sim 1400$. The roughness was composed of two-dimensional spanwise rods with a square cross-section that were periodically arranged in the streamwise direction with a pitch of $\lambda = 8k$. The roughness height was $k = 1.5\theta_{in}$, where θ_{in} is the momentum thickness at the inlet which corresponds to $k/\delta = 0.045 \sim 0.125$ and $k^+ = 32 \sim 45$, i.e. a very small ratio of roughness height to boundary layer thickness. In the simulation, the first rod was placed $80\theta_{in}$ downstream from the inlet; hence, at this location the surface condition changed abruptly from smooth to rough. The domain size along the streamwise direction was sufficiently long ($L_x = 768\theta_{in}$) for the flow to reach a new equilibrium state, creating a region where self-preservation was achieved. The rough-wall friction velocity was directly calculated from the total drag, which equals the sum of the skin-frictional and form drags. The virtual origin was defined as the distance to the centroid of the moment of forces acting on the rod roughness. The roughness effect was scrutinized by examining the profiles of the mean velocity, Reynolds stresses and higher-order statistics.

2. Numerical details

2.1. *Numerical procedure*

For an incompressible flow, the non-dimensional governing equations are

$$\frac{\partial u_i}{\partial x_i} = 0, \quad i = 1, 2, 3, \tag{1}$$

$$\frac{\partial u_i}{\partial t} + \frac{\partial}{\partial x_j} u_i u_j = -\frac{\partial p}{\partial x_i} + \frac{1}{Re} \frac{\partial^2 u_i}{\partial x_j \partial x_j} + f_i, \tag{2}$$

where x_i are the Cartesian coordinates and u_i are the corresponding velocity components. The free-stream velocity U_∞ and the momentum thickness at the inlet θ_{in} are used for non-dimensionalization. The Reynolds number is defined as $Re_\theta = U_\infty \theta_{in}/\nu$, where ν is the kinematic viscosity.

The governing equations (1) and (2) are integrated in time using the fully implicit fractional step method proposed by Kim, Baek & Sung (2002). All terms are advanced with the Crank–Nicholson method in time, and they are resolved with the second-order central difference scheme in space. Based on a block LU decomposition, both velocity–pressure decoupling and additional decoupling of the intermediate velocity components are achieved with the approximate factorization. Since the implicit decoupling procedure relieves the CFL restriction and the decoupled velocity components are solved without iteration, the computation time is reduced significantly. The immersed boundary method is used to efficiently describe the rough surface with Cartesian coordinates and a rectangular domain (Kim, Kim & Choi 2001). The discrete-time momentum forcing f_i is calculated explicitly in time to satisfy the no-slip condition on the immersed boundary using the previous velocity field near the forcing point. Linear and bilinear interpolation schemes are used to obtain the no-slip velocity at the immersed boundary when the forcing point does not coincide with the immersed boundary.

2.2. *Flow configuration*

Direct numerical simulations of the TBL over a rough or smooth wall were performed by means of a parallel computation using 32 CPUs of a supercomputer (IBM p690+). The domain size in the streamwise direction ($L_x = 768\theta_{in}$) was sufficiently long that the effects of the surface-roughness step change could be neglected. Since the rate of increase of the boundary layer thickness along the streamwise direction was smaller for the smooth wall than for the rough wall, the domain size along the streamwise direction for the smooth wall was chosen as twice that for the rough wall to obtain similar boundary layer thicknesses for both cases. The domain size along the wall-normal direction was tested for both $L_y = 60\theta_{in}$ and $90\theta_{in}$, and no significant differences were observed between the two cases; hence the smaller domain size, $L_y = 60\theta_{in}$, was chosen. The domain size along the spanwise direction was chosen as $L_z = 80\theta_{in}$, which was confirmed to be adequate based on the convergence of the spanwise correlation to zero at this domain size. The domain size and mesh resolution used in the present DNSs are summarized in table 1.

Realistic velocity fluctuations at the inlet were provided based on the method of Lund, Wu & Squires (1998). Before the main simulation, an auxiliary simulation was carried out to obtain the inflow data. The Reynolds number at the inlet for both cases was $Re_{\theta,in} = 300$. The convective outflow condition was used at the exit and the no-slip boundary condition was imposed at the solid wall. In the free stream, the conditions $u = U_\infty$ and $\partial v/\partial y = \partial w/\partial y = 0$ were imposed. Periodic boundary conditions were

	$Re_{\theta,in}$	L_x/θ_{in}	L_y/θ_{in}	L_z/θ_{in}	(N_x, N_y, N_z)	Δx^+	Δz^+	Δy^+_{min}	$\Delta t U_\infty/\theta_{in}$
Smooth	300	1536	60	80	(2049,150,257)	12.1	5.0	0.2	0.3
Rough	300	768	60	80	(2049,150,257)	6.0	5.0	0.2	0.1

TABLE 1. Domain size and mesh resolution.

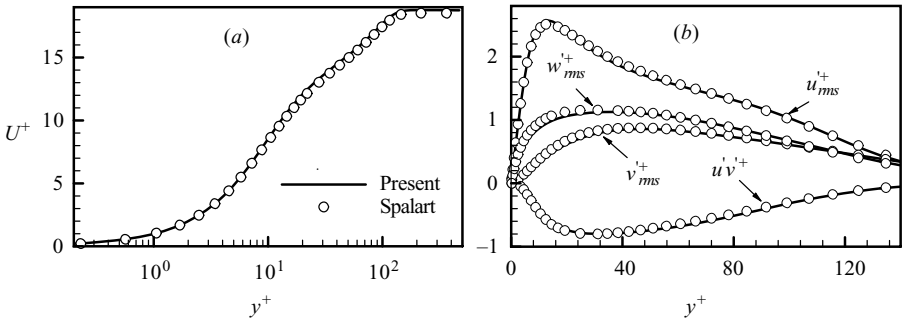

FIGURE 1. Inflow profiles at $Re_{\theta,in} = 300$. —, Present; ○, Spalart (1988).

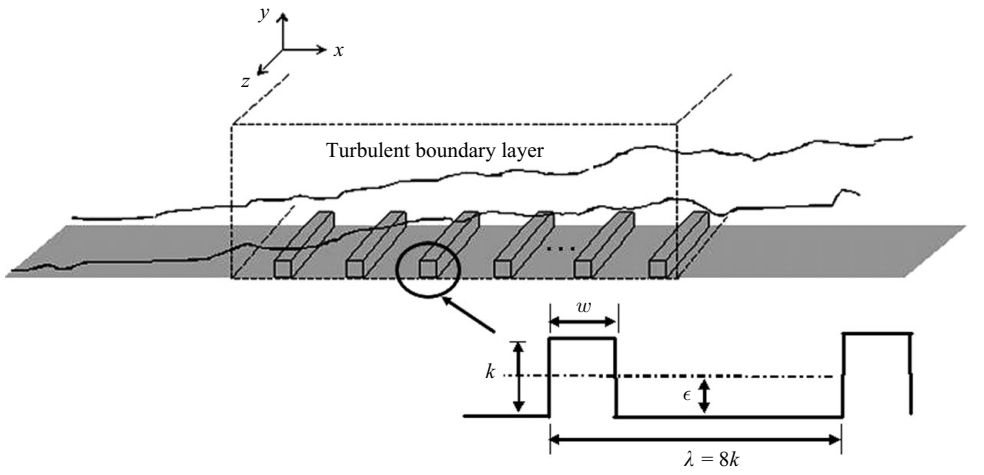

FIGURE 2. Schematic diagrams of computational domain and rod roughness. Only square rods ($w = k$) are considered.

used in the spanwise direction. To ascertain the reliability and accuracy of the present numerical simulation, the turbulence statistics were compared with the DNS data of Spalart (1988), as shown in figure 1. The mean velocity and turbulent stresses in the present results are in excellent agreement with those of Spalart (1988). A schematic diagram of the computational domain for the rough-wall case is shown in figure 2. The roughness takes the form of two-dimensional spanwise rods with a square cross-section that are periodically arranged in the streamwise direction with a pitch of $\lambda = 8k$. The roughness height is $k = 1.5\theta_{in}$, which corresponds to $k/\delta = 0.045 \sim 0.125$ and $k^+ = 32 \sim 45$. The first rod is placed $80\theta_{in}$ downstream from the inlet; the surface condition therefore changes abruptly from smooth to rough at this location, which is defined as $x = 0$.

3. Scaling parameters

Appropriate selection of the scaling parameters used to normalize velocity and length quantities is crucial to obtain a similarity profile of the rough-wall TBL or to compare flows generated under different conditions. A central issue when describing a rough-wall TBL is the accurate estimation of the friction velocity. For smooth-wall turbulent channel and boundary layer flows, a log-law profile is generally used to estimate the friction velocity. Using this approach, the friction velocity is easily obtained from the mean pressure gradient or total shear stress profile. Bakken *et al.* (2005) used this method to obtain the friction velocity in a symmetric rough-wall channel flow. However, it is not applicable to the rough-wall boundary layer flow considered here because the rough-wall boundary layer varies along the streamwise direction. The mean velocity profile in the whole boundary layer is generally used to estimate the friction velocity. The velocity distribution for the rough-wall TBL can be expressed in the following form:

$$U^+ = \frac{1}{\kappa}\ln y^+ + C - \Delta U^+ + \frac{2\Pi}{\kappa}\omega(\eta),$$

where $U^+ = U/u_\tau$, $y^+ = (y-\varepsilon)u_\tau/\nu$ and $\eta = (y-\varepsilon)/\delta$. Here, ε is the distance from the wall to the virtual origin, where y is measured from the bottom of the rough surface; κ is the Kármán constant; C is a smooth-wall constant; ΔU^+ is the roughness function; Π is the wake strength; and $\omega(\eta)$ is the wake function. Rewriting this equation in the following velocity-defect form simplifies the problem by reducing the number of unknown variables:

$$U_\infty^+ - U^+ = \frac{2\Pi}{\kappa}[\omega(1) - \omega(\eta)] - \frac{1}{\kappa}\ln\eta.$$

Krogstad *et al.* (1992) reported this formula, which optimizes parameters to fit the mean velocity profile in a velocity-defect form. The skin friction coefficient for a rough wall obtained by this method agreed well with that obtained by other methods. However, this method requires the optimization of three parameters and it has proved difficult to determine the friction velocity accurately in experiments on rough-wall TBLs.

In DNS, however, skin frictional drag and form drag can be directly calculated from wall shear stress and wall pressure data. The friction velocity can then be estimated from the total drag, which is the sum of the skin-frictional and form drags. This represents a strong advantage of DNS over experiment, since there is no ambiguity regarding the various parameters to fit. Leonardi *et al.* (2003) calculated the friction velocity using the total drag in a fully developed turbulent channel flow with a smooth upper wall and a lower wall with rod roughness elements. Since periodic boundary conditions along the streamwise direction can be used in a fully developed channel flow, both drags can be spatially averaged along the streamwise direction through the whole domain and the spatially averaged friction velocity has the same value at every position along the streamwise direction. In the present simulation, however, the boundary layer is spatially developing and periodic boundary conditions cannot be applied along the streamwise direction. Hence, instead of averaging along the streamwise direction through the whole domain, the skin frictional drag and form drag are spatially averaged over one pitch λ, that is, the distance between adjacent rods.

The spatially averaged skin-frictional drag (C_f) and form drag (P_d) are shown in figure 3(*a*). The skin-frictional drag decreases near the step change ($x = 0$) and is

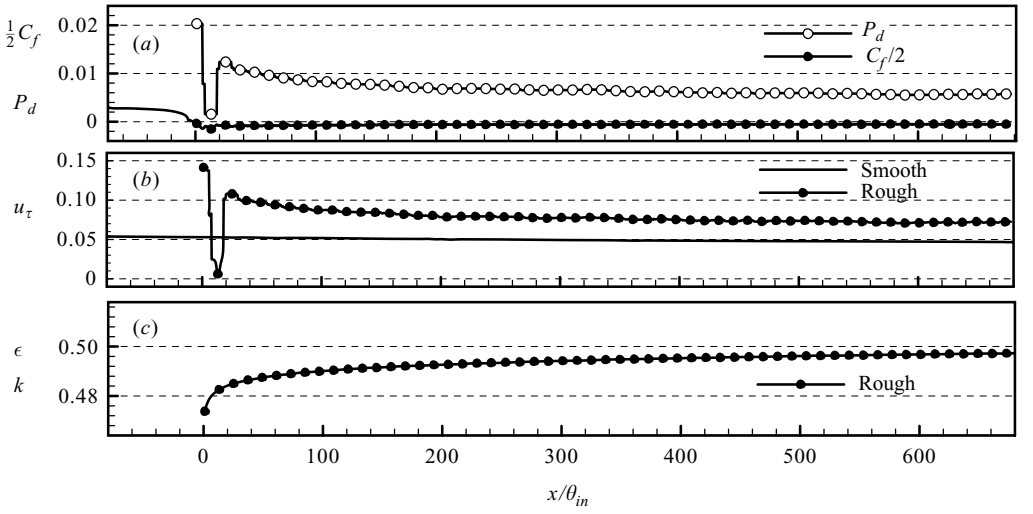

FIGURE 3. Variations of spatially averaged (*a*) skin-frictional drag, (*b*) form drag, friction velocity and (*c*) virtual origin along streamwise direction. Each circle represents a center position of each rod.

negative over the rough wall. It exhibits a very large positive value directly above each rod, and a negative value within the cavity, where a large recirculation region with two vortices exists. The spatially averaged skin-frictional drag within the cavity is negative because the cavity is 7 times longer than the rod width. Since the form drag induced by the pressure difference between the upstream and downstream vertical walls of the rod is much larger than the skin-frictional drag, the total drag is larger than that of a smooth wall in spite of the negative skin-frictional drag. Figure 3(*b*) shows the variations of friction velocity along the streamwise direction for the smooth and rough walls. The friction velocity of the rough wall abruptly increases just upstream of the step change in the roughness and decreases after the first rod. This decrease is due to the very small form drag that is induced by the first rod. The first rod induces a very large recirculation and a reduced pressure within the cavity. After the second rod, the friction velocity increases again and then decreases slowly, converging to a constant value. In the present study, the friction velocity of the rough wall converged to a constant value at about $x > 300\theta_{in}$, which corresponds to 30 times the boundary layer thickness at the first rod. Antonia & Luxton (1971), by contrast, observed that the skin friction adjusted to a new rough wall within 3 or 4 boundary layer thicknesses, which is much smaller than the distance observed in the present DNS. This discrepancy may be due to the small ratio of boundary thickness to the first rod roughness height in the present DNS ($\delta/k = 6.7$).

The wall-normal distance (y) from the wall can be clearly defined for the flow with a smooth wall. However, the origin of y in a rough wall is ambiguous owing to the complex wall geometry. Typically, the origin of y in a rough wall has been defined using a fitting method based on lag-law of mean velocity profiles. As an alternative to this method, Jackson (1981) defined the distance (ε) from the bottom wall to the virtual origin as the distance to the centroid of the moment of the forces acting on the rod roughness. Figure 3(*c*) shows the variation of the distance from the bottom wall to the virtual origin (ε) along the downstream direction. The distance to the virtual origin is almost about half of the roughness height (k), and its variation along

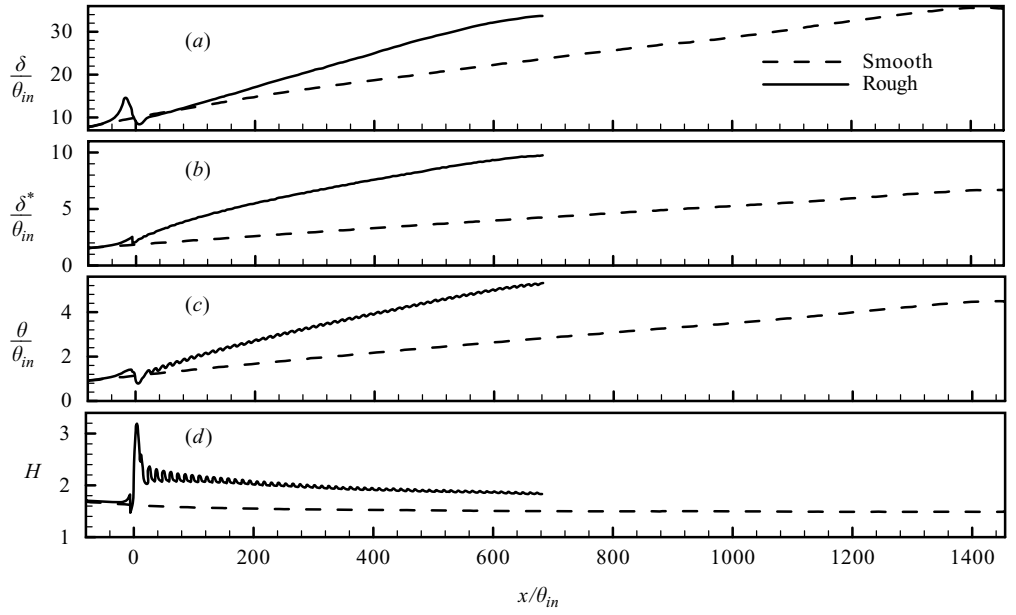

FIGURE 4. Variations of (*a*) boundary layer thickness, (*b*) displacement thickness, (*c*) momentum thickness and (*d*) shape parameter in the downstream direction.

streamwise direction is very small. In the present DNS, $y' = y - \varepsilon$ is defined as the distance from the virtual origin.

Figure 4 shows the variations of the boundary layer thickness, displacement thickness, momentum thickness, and shape parameter after the roughness step change along the streamwise direction. The boundary layer thickness (δ) increases almost linearly along the streamwise direction for both the rough and smooth walls, with the rough wall showing a larger rate of increase. The integral length scales (δ^* and θ) of the rough wall are also larger than those of the smooth wall. The shape factor (H) of the rough wall increases significantly near the step change and converges on moving downstream. The increase of the displacement thickness is more pronounced for the rough wall and the converged shape factor of the rough wall is larger than that of the smooth wall. These different growth rates with outer length scales after the roughness step change along the streamwise direction may show the existence of a self-preserving form in the outer layer.

4. Self-preservation of the rough-wall turbulent boundary layer

In order to simulate a spatially developing rough-wall TBL, an abrupt surface roughness change is necessary. In contrast to fully developed rough-wall channel flow, the rough-wall boundary layer varies along the streamwise direction. The direct generation of a turbulent inflow that realistically reflects various surface roughness conditions is impossible. Accordingly, the inflow condition of a smooth wall is provided at the initial stage and then a roughness step change is imposed at some position downstream ($80\theta_{in}$ in the present work), where a fully developed smooth boundary layer is obtained. Figure 5 shows contour plots in the (x, y)-plane of the velocity and pressure fluctuations in the step change region. The velocity and pressure fluctuations are

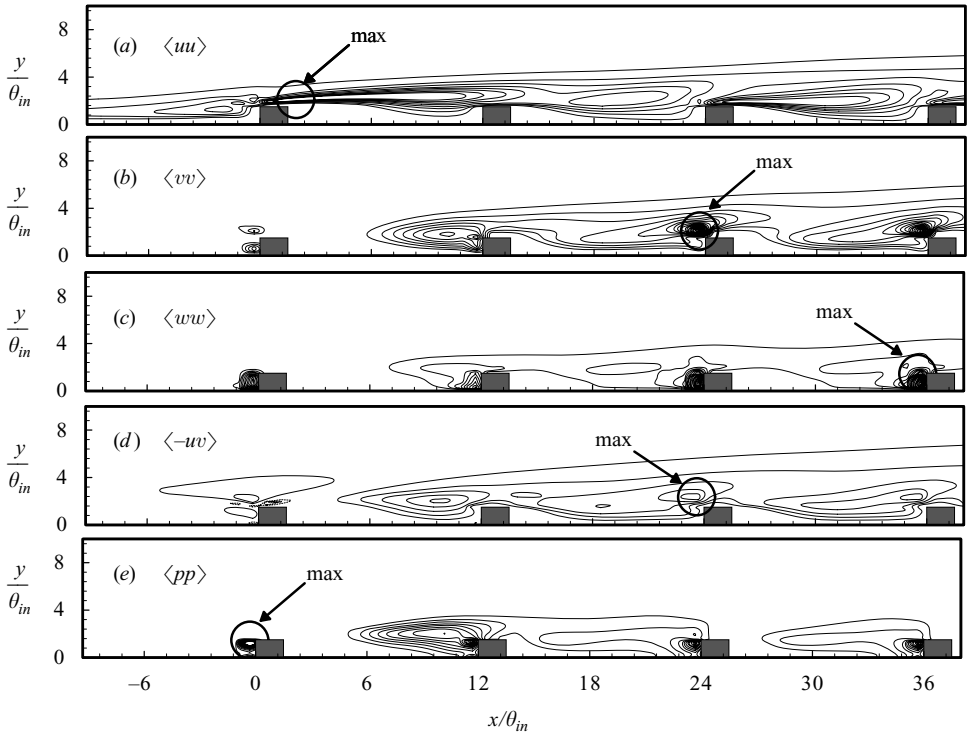

FIGURE 5. Variations of velocity and pressure fluctuations near the roughness step change region. Dashed lines denote the regions of negative value.

significantly increased in the vicinity of the first four rods and slowly converge on moving downstream. Near the crest of the first rod, there is a very small region where turbulent shear stress $-\langle uv\rangle$ has a negative value. After the step change, there is a transient region in which the flow adapts to the new boundary conditions. In the present DNS of a rough-wall TBL, the domain size along the streamwise direction should be sufficiently large to reach a new equilibrium state where a self-preserving form is achieved.

Smalley, Antonia & Djenidi (2001) proposed two conditions for self-preservation in a rough-wall TBL: the friction velocity should be constant along the streamwise direction; and the boundary layer thickness should increase linearly along the streamwise direction. In the present simulation, the friction velocity converges to a constant value at about $x > 300\theta_{in}$ and the boundary layer thickness increases almost linearly in this region, indicating that self-preservation can be achieved at about $x > 300\theta_{in}$. The velocity-defect profiles at various locations along the streamwise direction are shown in figure 6. Note that the velocity is normalized by the friction velocity and boundary layer thickness. For $x > 132\theta_{in}$, the velocity-defect profiles become almost identical, indicating that self-preservation has been established.

Figures 7 and 8 show the variations of the Reynolds stress in the inner and outer layers along the streamwise direction, which are normalized by the inner length scale $y^+ = y'u_\tau/\nu$ and the outer length scale y'/δ, respectively. Figure 7 shows that, after normalization by the friction velocity, the peak values of $\langle u^{+2}\rangle$ and $\langle w^{+2}\rangle$ increase and those of $\langle v^{+2}\rangle$ and $\langle -u^+v^+\rangle$ decrease on moving downstream. These trends are due to the fact that the rate of decrease of the Reynolds stress in the inner layer is

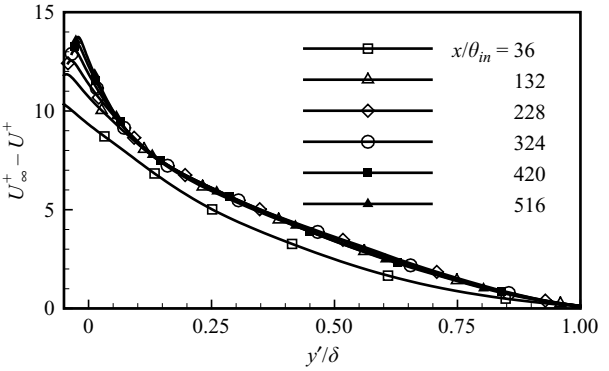

FIGURE 6. Variations of streamwise mean velocity in the downstream direction.

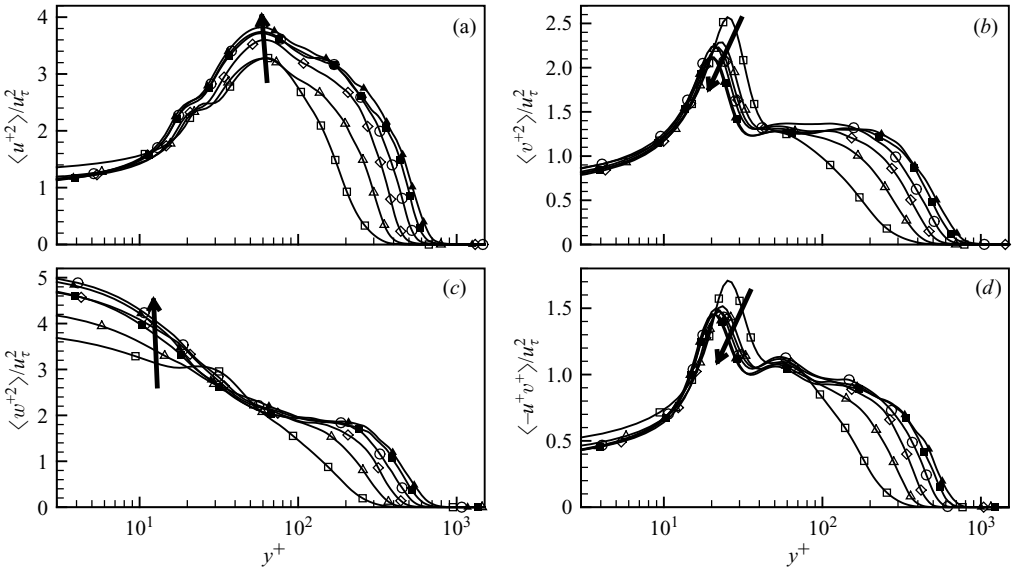

FIGURE 7. Variations of turbulent Reynolds stresses in the direction downstream in the inner coordinates, normalized by u_τ^2. Symbols as in figure 6.

different from that of the friction velocity on moving downstream. After $x = 324\theta_{in}$, the two rates of decrease are almost the same, indicating that the flow is close to an equilibrium state. The profiles of the Reynolds stress collapse well in the inner layer when they are normalized by the inner length scale. In this region, the peak values are located at the same height in wall units. The peak of $\langle u^{+2}\rangle$ is located at $y^+ = 55$, which is about $2 \sim 2.5$ times the roughness height. For $\langle v^{+2}\rangle$, the peak is located at $y^+ = 20$, which is about 1.1 times the roughness height. The peak of $\langle w^{+2}\rangle$ is located at $y^+ = 0$, which is the height of the virtual origin and about half of the roughness height. The peak of $\langle -u^+v^+\rangle$ is located at a position similar to that of $\langle v^{+2}\rangle$. Figure 8 shows that the Reynolds stresses in the outer layer increase on moving downstream. This increase can be attributed to the presence of the roughness step change, which causes a large increase in turbulent fluctuations near the wall that then propagate to the outer layer as the flow moves downstream. Self-preservation is obtained in the

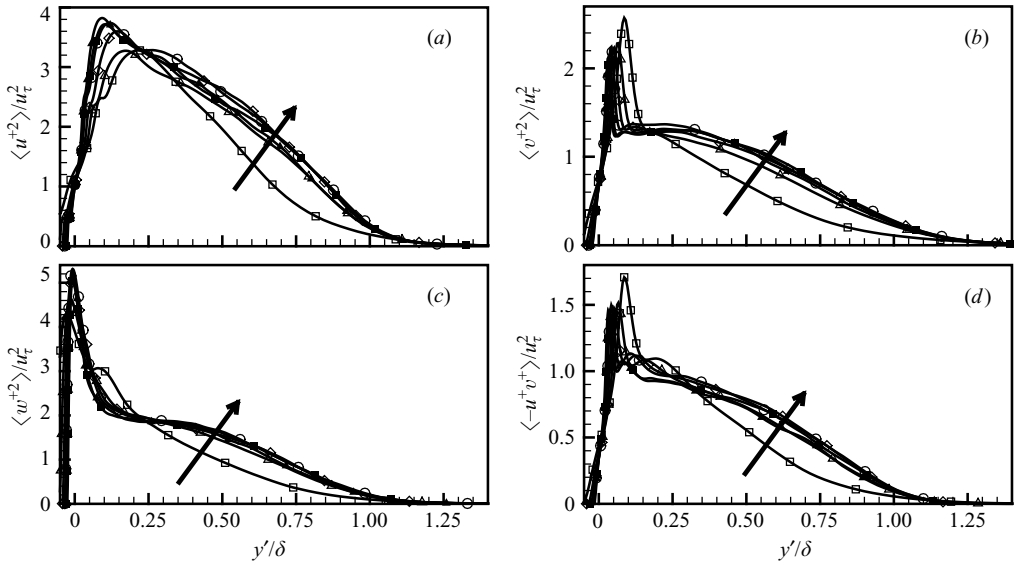

FIGURE 8. Variations of turbulent Reynolds stresses along the downstream in the outer coordinates, normalized by u_τ^2. Symbols as in figure 6.

outer layer after $x = 324\theta_{in}$ when normalized by the boundary layer thickness as the outer length scale.

5. Roughness sublayer

Introduction of the rod roughness elements onto the smooth surface significantly affects the turbulent flow structures, leading to very high turbulent intensities in the vicinity of the wall. This near-wall region, which is known as the roughness sublayer, is generally assumed to have a height of $2 \sim 5$ times the roughness height. The limit of the roughness sublayer is defined as the point at which the turbulence statistics become spatially homogeneous (Bhaganagar *et al.* 2004). Iso-contours of mean quantities in the roughness sublayer are displayed in figure 9, where a new coordinate origin is defined as $s = 0$ at $x = 516\theta_{in}$ (i.e. at the leading-edge of the 44th rod) and the next rod is defined as $s = 8$. The streamline iso-contours in figure 9(a) are very similar to those reported by Ashrafian *et al.* (2004). Two recirculation zones, with focal points at $(s, y/k) = (3.2, 0.75)$ and $(7.5, 0.3)$, are observed in the cavity between the two consecutive rods. Owing to these recirculation regions, the streamwise mean velocity is negative above the entire length of the cavity wall and there is no reattachment point. Above the crest, the streamwise mean velocity gradient is very high, which increases the production of turbulent kinetic energy. In front of the leading edge of the rod, the wall-normal mean velocity is increased near the crest and negative near the wall. At the centre of the cavity, the wall-normal velocity is negative due to flow entrainment. The mean pressure has a minimum value near the centre of the first recirculation region and a maximum value in front of the leading vertical wall. A large pressure difference is observed between the two vertical walls of each rod, which produces a high form drag.

Figure 10 shows iso-contours of velocity and pressure fluctuations in the roughness sublayer. The streamwise velocity fluctuations are increased above the crest and have a maximum value at $(s, y/k) = (4, 1.5)$. The wall-normal velocity fluctuations are

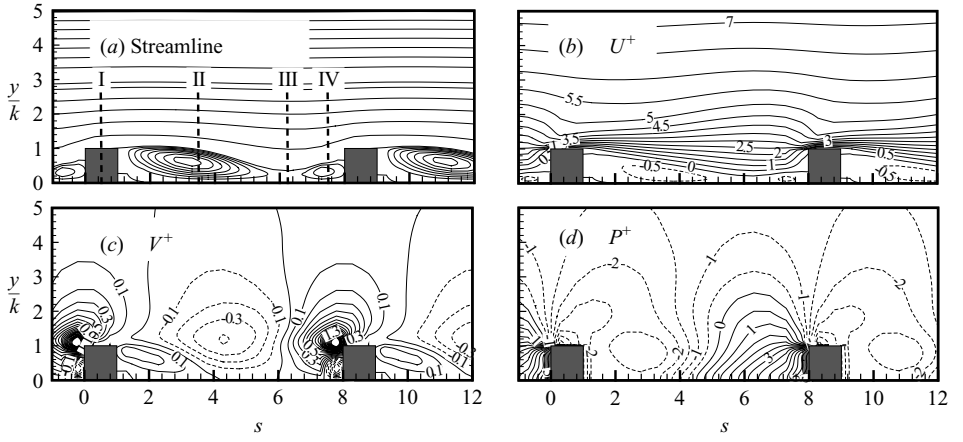

FIGURE 9. Iso-contours of mean quantities in the roughness sublayer.

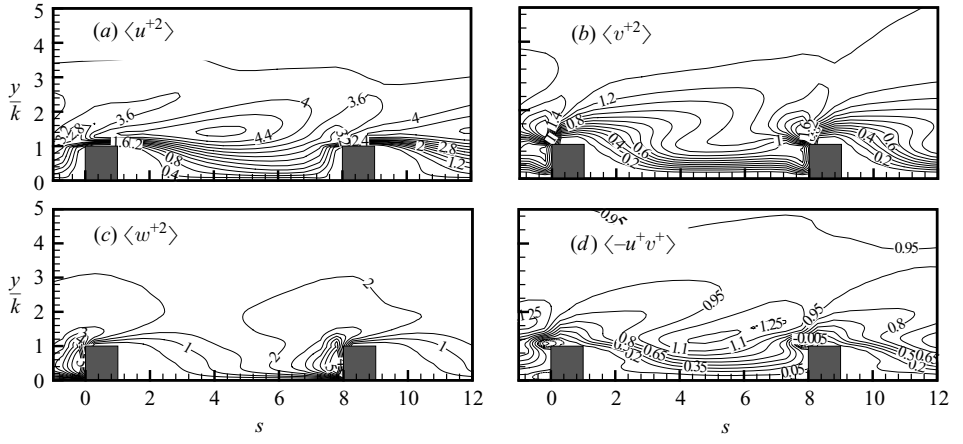

FIGURE 10. Iso-contours of velocity and pressure fluctuations in the roughness sublayer. Dashed lines denote the regions of negative value.

increased above the leading edge of the rod and the spanwise velocity fluctuations are very high in front of the leading edge of the rod at $y/k = 0.5$, indicating that the streamwise velocity fluctuations are distributed in the spanwise direction in the region of $y < k$ and in the wall-normal direction in the region of $y > k$ owing to the blockage effect of the rod roughness. The Reynolds shear stress is increased above the cavity ($s = 5$) and near the leading edge ($s = 7$), where sweep and ejection events are very active. In front of the leading edge, there are small regions where the Reynolds shear stress has a negative value. This is in good agreement with the DNS results of turbulent channel flow with a rough wall by Ashrafian & Andersson (2006*b*).

Figure 11(*a–l*) shows the profiles of flow quantities at the four locations (I) ~ (IV) marked in figure 9(*a*). The four locations are the same as those selected by Ashrafian *et al.* (2004): I, the centre of the roughness crest ($s = 0.5$); II, near the focal point of the first recirculation zone ($s = 3.5$); III, the saddle point between the two recirculation zones ($s = 6.25$); and IV, the focal point of the second recirculation zone ($s = 7.5$). For all of the flow quantities except the wall-normal mean velocity, the profiles at locations (I) ~ (IV) are indistinguishable above $y = 5k$. In the case of the wall-normal

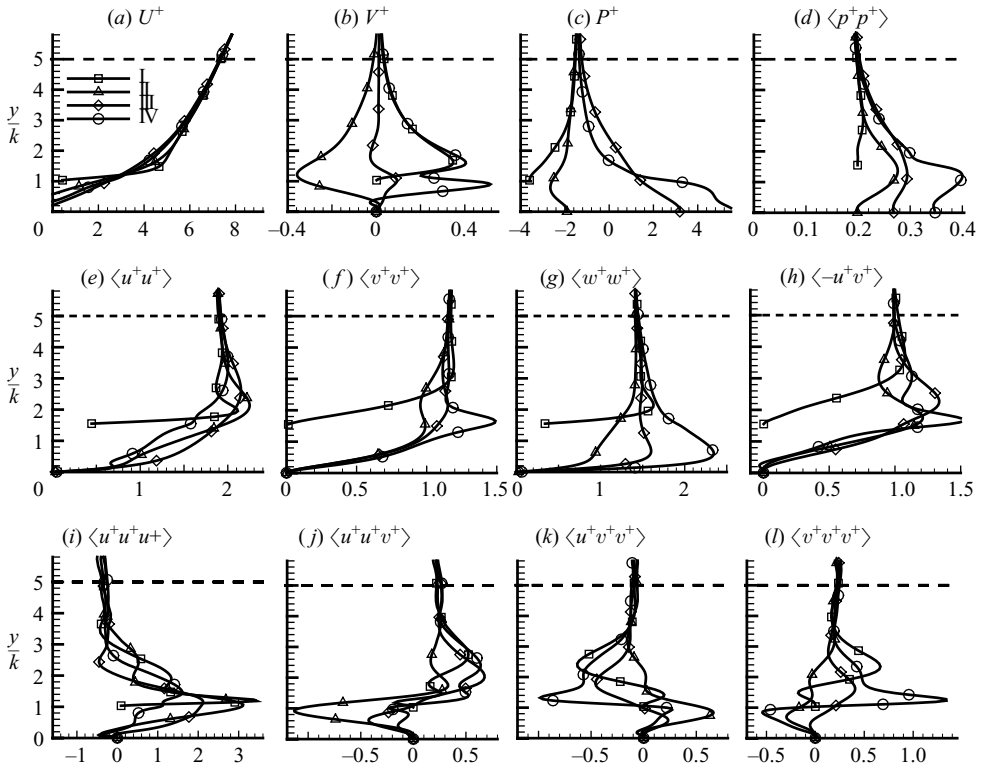

FIGURE 11. Variations of velocities and pressure at locations I∼IV in the roughness sublayer.

mean velocity, a slightly inhomogeneous region is observed in the region $y < 6k$. These results thus indicate that the roughness sublayer is located in the region $y < 5k$ and the outer-layer region is above $y = 5k$.

6. Comparison of the rough and smooth walls

Many previous experimental studies have found that the turbulent stresses outside the roughness sublayer are independent of the surface roughness, i.e. the Townsend wall similarity hypothesis (Raupach *et al.* 1991; Flack *et al.* 2005). In a study of TBL, however, Krogstad *et al.* (1992) and Krogstad & Antonia (1999) found that the turbulent stresses were affected by the roughness and that the interaction between the inner and outer layers was not weak. In the present study, the effect of roughness is examined by comparing the characteristics of TBLs over smooth and rough walls. For this comparison, all the data for the rough-wall turbulent boundary layer were obtained at a location sufficiently downstream ($x = 516\theta_{in}$) that the flow had achieved a steady state. At this point, the thickness of the roughness sublayer is estimated to be $y = 5k$. Within the roughness sublayer, turbulence statistics were obtained at locations II and IV marked in figure 9(*a*). The smooth-wall data were obtained at $x = 1068\theta_{in}$, where the boundary layer thickness is the same as that of the rough wall at $x = 516\theta_{in}$. The Reynolds number based on the momentum thickness Re_θ is 1351 for the rough wall and 1098 for the smooth wall. The friction velocity normalized by the free-stream velocity is 0.0735 for the rough wall and 0.0445 for the smooth wall, and the roughness Reynolds number $k^+ = ku_\tau/\nu$ is 33.1.

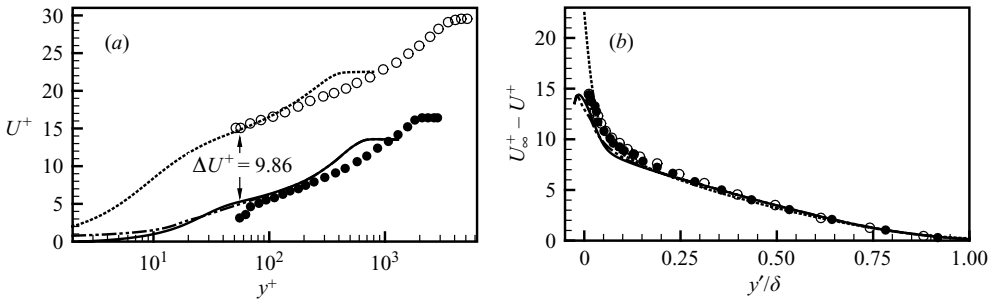

FIGURE 12. Mean velocity profiles. Present DNS: ---, smooth wall; —, rod roughness at location II; –··–, rod roughness at location IV. Krogstad & Antonia (1999): ○, smooth wall; ●, rod roughness.

6.1. *Mean velocity*

The mean streamwise velocity profiles for smooth and rough walls are shown in figure 12. The experimental data of Krogstad & Antonia (1999) are included for comparison. The general mean velocity shift (ΔU^+) is clearly shown and is estimated to be 9.86. Krogstad & Antonia (1999) suggested that for k-type roughness, ΔU^+ and k^+ are related by a logarithmic function of the form $\Delta U^+ = (1/\kappa)\ln k^+ + 1.2$. If we use this formula, the predicted roughness function is $\Delta U^+ = 9.73$, which is slightly smaller than the value obtained in the present DNS. This difference may be due to the different rod roughness employed: the present work uses square rods with a pitch to height ratio of $\lambda/k = 8$, where as Krogstad & Antonia (1999) used circular rods with $\lambda/k = 4$. The two results can be compared in terms of the effective sand-grain roughness height k_s, which can be calculated from $\Delta U^+ = (1/\kappa)\ln k_s^+ - 3.2$ (Raupach *et al.* 1991). According to this relation, the present rod roughness is $k_s^+ = 211.5$. The ratio k_s/k is 6.39, which is similar to that of Krogstad & Antonia (1999). The velocity-defect profiles, displayed in figure 12(*b*), show very good agreement between the present DNS results and the experimental data of Krogstad & Antonia (1999). In the outer layer, the velocity-defect profiles of the smooth and rough walls collapse well and show good surface similarity.

6.2. *Reynolds stresses*

The Reynolds stresses normalized by u_τ^2 are compared in figure 13 for the smooth and rough walls. The experimental data of Krogstad & Antonia (1999) are also included for comparison. In this figure, a dashed vertical line is used to mark the boundary between the outer layer ($y > 5k$) and the roughness sublayer ($y < 5k$). In the plots of the streamwise normal stress $\langle u^{+2}\rangle$ (figure 13*a*), the peak in the roughness sublayer is considerably weaker in the rough-wall case compared to the smooth-wall case owing to the blockage effect of the rod roughness, especially near the leading edge (location IV). In the outer layer, however, $\langle u^{+2}\rangle$ for the rough wall case becomes greater than that of the smooth wall case. These trends are in good agreement with the experimental data of Krogstad & Antonia (1999). The wall-normal stresses $\langle v^{+2}\rangle$ (figure 13*b*), by contrast, are higher in the rough- than in the smooth-wall case in both the roughness sublayer and the outer layer, although the increase of $\langle v^{+2}\rangle$ in the outer layer is smaller than that observed by Krogstad & Antonia (1999). The spanwise normal stresses $\langle w^{+2}\rangle$ and Reynolds shear stresses $\langle -u^+v^+\rangle$ (figures 13*c* and 13*d* respectively) exhibit a similar increase in the outer layer. Near the leading edge (location IV), the near-wall peaks of $\langle v^{+2}\rangle$, $\langle w^{+2}\rangle$ and $\langle -u^+v^+\rangle$ are significantly

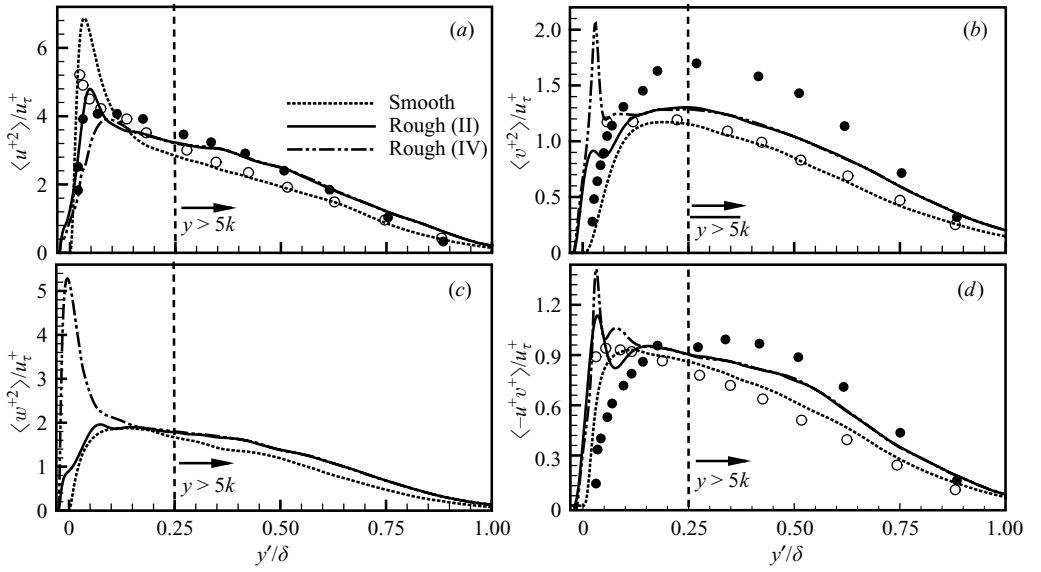

FIGURE 13. Reynolds stresses in the outer coordinates, normalized by u_τ^2. Symbols as figure 12.

higher for the rough wall than for the smooth wall. The present results are in good agreement with the experimental data of Krogstad & Antonia (1999). Consistent with the findings of these experiments, our results indicate that the introduction of surface roughness affects the turbulent Reynolds stresses outside the roughness sublayer.

As outlined above (figure 12*b*), the velocity-defect form for the smooth and rough walls shows good similarity in the outer layer. Similar results are obtained for other outer variables, such as the displacement thickness and momentum thickness. However, the Reynolds stress profiles normalized by the friction velocity do not show good similarity between the rough- and smooth-wall cases. Jimenez (2004) suggested that δ/k must be larger than 40 before wall similarity can be expected. However, δ/k used in this study is about $8 \sim 22$. Schultz & Flack (2005) proposed that k_s is a better representative length scale than k for comparing roughness effects with different roughness geometrical characteristics, and that the extent of the roughness sublayer is $5k_s$ rather than $5k$. They conjectured that the turbulence structure will be changed when the extent of the roughness sublayer is larger than the inner layer itself ($5k_s > 0.2\delta$). In the present DNS study, $5k$ is equal to about 0.25δ and $5k_s$ to about 1.59δ, which is larger than their criterion. However, the above criterion should be further investigated to see whether it can be applied to all flow types and roughness types generally. For example, a DNS study by Ashrafian *et al.* (2004) of turbulent channel flow with the same two-dimensional rod-roughened wall used the roughness height of $h/k = 29.4$ and $5k_s = 0.82h$, where h is the channel half-width. They are slightly smaller than the present roughness height but still much higher than the criterion of Jimenez (2004) and Schultz & Flack (2005). Despite this, however, Ashrafian *et al.* (2004) reported the existence of wall similarity between the flows over smooth and rough walls, indicative of a very weak interaction between the inner and outer layers. These findings thus indicate that the above criterion is not universal to all flow types (e.g. channel flow and boundary layer) and the lack of wall similarity is not only due to the large roughness height but also the characteristics of

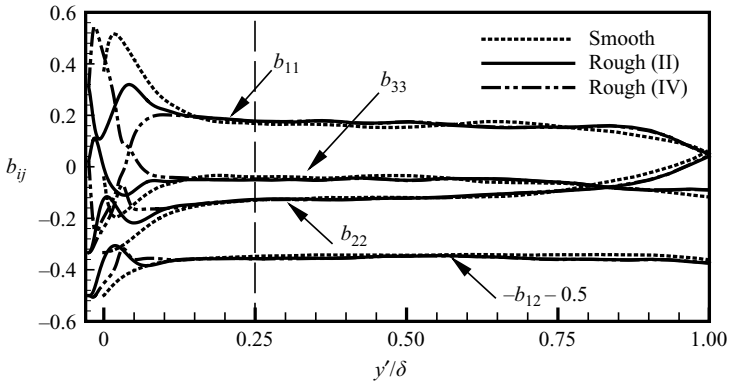

FIGURE 14. Anisotropy tensors in the outer coordinates. Note that $-b_{12}$ is shifted downwards by 0.5 to avoid crowding: - - -, smooth wall; —, rod roughness at location II. – · · –, rod roughness at location IV.

turbulent boundary layer. This also supports the conjecture of Krogstad *et al.* (2005) that surface roughness effects on the outer layer depends on the outer boundary condition.

6.3. *Reynolds stress anisotropy*

The Reynolds stress anisotropy tensor is free from the error associated with estimating the friction velocity. The anisotropy tensor is defined as

$$b_{ij} = \frac{\langle u_i u_j \rangle}{q^2} - \frac{1}{3}\delta_{ij},$$

where $q^2 = \langle u_l u_l \rangle$ and δ_{ij} is the Kronecker delta. Several previous experimental studies have shown that the introduction of surface roughness causes a reduction in the anisotropy tensor throughout the boundary layer (e.g. Krogstad & Antonia 1994; Shafi & Antonia 1995; Djenidi, Elavarasan & Antonia 1999; Antonia & Krogstad 2001; Keirsbulck *et al.* 2002*b*). In a comparison of anisotropy tensors between smooth and rough walls using various previous experimental and numerical data, Smalley *et al.* (2002) found that the magnitudes of b_{11}, b_{22} and b_{33} for the rod-roughened wall are decreased more than those of the smooth wall in the outer layer. Leonardi *et al.* (2003) showed a general reduction of the anisotropy tensor when rod roughness was introduced onto one side wall of a channel. These results indicate that the presence of roughness can lead to a more even distribution of turbulent energy among the three components for both boundary layer and channel flows. On the contrary, Mazouz, Labraga & Tournier (1998) and Sabot, Saleh & Compte-Bellot (1977) found that the anisotropy is increased by the introduction of k-type rod roughness across an entire channel or pipe. Ashrafian & Andersson (2006*a*) observed no difference in the anisotropy in the outer layers of channels with smooth walls and those with two-dimensional rod roughness. These results indicate that anisotropy is strongly related to the flow type and roughness used.

The profiles of the Reynolds anisotropy tensors b_{ij}, displayed in figure 14, show that the introduction of rod roughness significantly reduces the anisotropy within the roughness sublayer. The increase of b_{33} within the cavity near the bottom wall ($y/k < 0.5$) between consecutive rods is markedly stronger than that of b_{22}. This may be due to the redistribution of the turbulent energy from the wall-normal direction to the streamwise and spanwise directions. In the roughness sublayer ($y/\delta < 0.25$),

the decrease of b_{11} and increase of b_{22} and b_{33} are prominent near the leading edge (location IV), indicating that the turbulent energy is transferred from the streamwise direction to the wall-normal and spanwise directions owing to the blockage effect of the rod roughness. This redistribution of turbulent energy is very similar to that of DNS for rough-wall channel flow by Ashrafian & Andersson (2006*b*). They provided detailed information on redistribution of turbulent energy by using the velocity–pressure gradient. Note that roughness effects on turbulent Reynolds stresses and turbulent energy redistribution within the roughness sublayer are very similar for channel flow and boundary layers. In the outer layer, the introduction of surface roughness has little effect on the Reynolds anisotropy tensor. This finding differs from most previous experimental results, but is similar to the behaviour observed in a DNS of turbulent channel flow (Krogstad *et al.* 2005), which showed no discernible difference in the Reynolds anisotropy tensor in the outer layer ($y > 5k$) between the smooth and rough cases. As shown in figure 13, the surface similarity hypothesis is not satisfied for the Reynolds stresses. However, the Reynolds stress anisotropy tensors show good surface similarity in the outer layer. Although the increased production of turbulent kinetic energy in the vicinity of the rough wall causes an increase in the Reynolds stresses, no significant contribution is made to the relative magnitude of the different tensor components. This suggests that the turbulent energy is redistributed from $\langle u^{+2} \rangle$ to $\langle v^{+2} \rangle$ and $\langle w^{+2} \rangle$ in the roughness sublayer rather than in the outer layer.

6.4. *Third-order turbulence statistics*

Velocity triple products are likely to be more sensitive to surface roughness than second-order statistics due to their higher degree of nonlinearity. Hence velocity triple products may be useful in elucidating the modification of the turbulent transport processes that occurs when roughness is added to a smooth wall. However, the large uncertainties involved in measuring these triple products mean that relatively few experimental data are available compared with those for the first- and second-order turbulence statistics. Andreopoulos & Bradshaw (1981) reported that applying sandpaper to a smooth wall significantly altered the velocity triple products out to a distance of up to 10 roughness heights above the surface. Bandyopadhyay & Watson (1998), Krogstad & Antonia (1999) and Antonia & Krogstad (2001) examined the effects of surface roughness on high-order turbulence statistics in the outer layer. Bhaganagar *et al.* (2004) performed a DNS of turbulent channel flow with three-dimensional regular roughness on the bottom wall, and showed that the skewness of the velocity fluctuation is significantly affected in the outer layer by the surface roughness. On the other hand, experiments by Schultz & Flack (2005) on a boundary layer and a DNS of a turbulent channel flow by Ashrafian & Andersson (2006*a*) showed that the surface roughness effects on high-order turbulence statistics are restricted to inside the roughness sublayer and are negligible in the outer layer. Figure 15(*a–d*) shows profiles of the velocity triple products of fluctuating components $\langle u^{+3} \rangle$, $\langle u^{+2} v^{+} \rangle$, $\langle u^{+} v^{+2} \rangle$ and $\langle v^{+3} \rangle$, normalized by u_τ^3, for smooth and rough walls. The experimental data of Krogstad & Antonia (1999) and Keirsbulck *et al.* (2002*a*) are included for comparison. Outside the roughness sublayer, the simulation and experimental data are in good agreement. In addition, the present data are in good agreement with those of Ashrafian & Andersson (2006*b*) within the roughness sublayer (not shown here).

The present rough-wall DNS data for $\langle u^{+3} \rangle$ differ only slightly from the smooth-wall data in the region $y/\delta > 0.25$, but differ markedly in the region $y/\delta < 0.25$. For

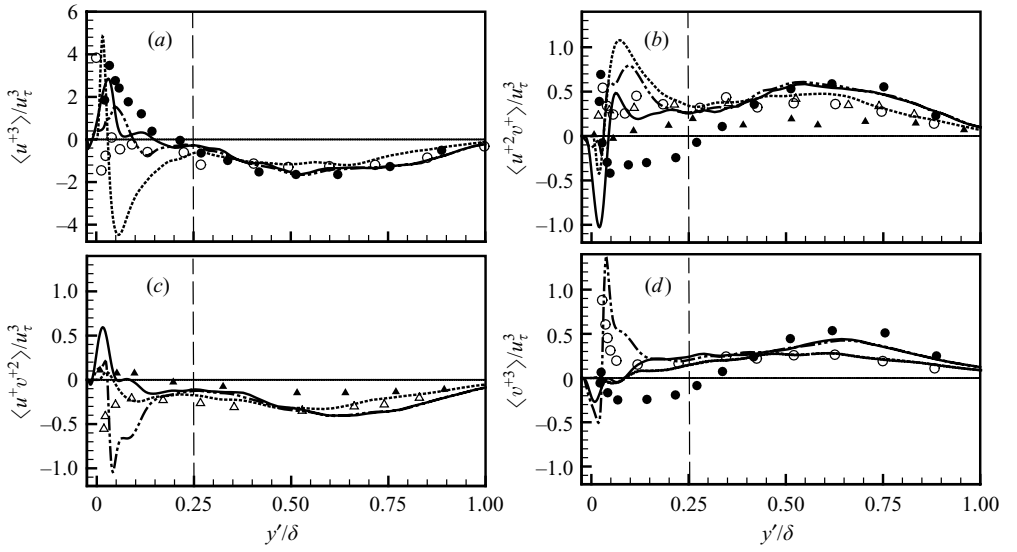

FIGURE 15. Velocity triple products in the outer coordinates, normalized by u_τ^3: - - -, smooth wall; —, rod roughness at location II; – · –, rod roughness at location IV (Present DNS); ○, smooth wall; ●, rod roughness (Krogstad & Antonia 1999); △, smooth wall; ▲, rod roughness (Keirsbulck *et al.* 2002*a*).

the rough wall, the positive peak of $\langle u^{+3}\rangle$ near the wall is less intense and moves outwards, and the negative peak disappears. The positive peak at location IV (i.e., near the leading edge) is significantly reduced, which may be related to the partial break-up of the streamwise vortices by the roughness elements. For the smooth wall, $\langle u^{+3}\rangle$ changes from positive to negative at about $y/\delta = 0.03$ ($y^+ \approx 13.5$), whereas for the rough wall this sign change occurs farther from the wall, at $y/\delta = 0.1\sim0.14$ ($y^+ \approx 68\sim92$), indicating that sweep motions ($u' > 0$, $v' < 0$) are stronger near the rough wall than the smooth wall. This may be due to the less strict wall-normal boundary condition for the rough wall, which would allow a greater amount of high-momentum fluid to be swept into the cavity between the rods. These findings are in agreement with the observations of Grass, Stuart & Mansour-Tehrani (1993), who investigated energetic inrush events towards a wall with k-type strip roughness, and are consistent with the results of rough-wall boundary layer experiments of Bisceglia *et al.* (2001), Krogstad & Antonia (1999), Keirsbulck *et al.* (2002*a*) and Schultz & Flack (2005). In the present simulations, the increased sweep event is strong near the center of the cavity (location II) and weak near the leading edge (location IV), where the Reynolds shear stress has a maximum value in the roughness sublayer (see figure 10*d*). Krogstad & Antonia (1999) showed a positive peak of $\langle v^{+3}\rangle$ in the vicinity of the wall, but no such peak was observed in the present smooth-wall DNS, nor in a previous DNS of turbulent channel flow (Ashrafian & Andersson 2006*a*). For the rough wall, $\langle v^{+3}\rangle$ has a negative peak in the cavity ($y < k$) whose position coincides with the focal point of two recirculation zones (locations II and IV) from the increased sweep events towards the cavity. Outside the cavity ($y > k$), $\langle v^{+3}\rangle$ is positive and wall-normal velocity fluctuations are transported outward from the wall. In particular, a very large positive peak is observed at location IV, indicating that ejection events are very strong above the leading edge.

The triple products $\langle u^{+2}v^{+}\rangle$ and $\langle u^{+}v^{+2}\rangle$ represent the wall-normal turbulent transport of $\langle u^{+2}\rangle$ and $\langle -u^{+}v^{+}\rangle$, and their gradients along the wall-normal direction represent the turbulent diffusion in the Reynolds stress transport equation. In figure 15(b, c) $\langle u^{+2}v^{+}\rangle$ is decreased and $\langle u^{+}v^{+2}\rangle$ is increased in the cavity region ($y < k$). The negative peak of $\langle u^{+2}v^{+}\rangle$ and positive peak of $\langle u^{+}v^{+2}\rangle$ are very strong at $y/\delta \approx 0.025$ at location II and weak at location IV, indicating that strong wall-ward transport of $\langle u^{+2}\rangle$ and $\langle u^{+}v^{+}\rangle$ occurs at location II and strong outward transport at location IV due to the increased sweep and ejection events. In the outer layer, the slope of $\langle u^{+2}v^{+}\rangle$ for the rough wall is positive and larger than that of the smooth wall in the region $0.25 < y/\delta < 0.64$, and the sign changes at $y/\delta \approx 0.64$. In the profiles of $\langle u^{+}v^{+2}\rangle$ and $\langle v^{+3}\rangle$, the slope is increased in the same region. This indicates that there is a loss of kinetic energy due to transport of this energy away from the wall and that the loss is larger for the rough wall than for the smooth wall. This is consistent with the experimental results of Krogstad & Antonia (1999) for TBLs. In the region $y/\delta > 0.5$, the wall-normal turbulent transport of $\langle u^{+2}\rangle$, $\langle -u^{+}v^{+}\rangle$ and $\langle v^{+2}\rangle$ (i.e. the profiles of $\langle u^{+2}v^{+}\rangle$, $\langle u^{+}v^{+2}\rangle$ and $\langle v^{+3}\rangle$) is in the outward direction for the rough wall to a greater extent than for the smooth wall. The data for turbulent channel flow with smooth and rough walls showed that on going from a smooth to a rough wall, there was only a gain in the kinetic energy transported from the wall, with no change in the sign of the slope (Bakken *et al.* 2005; Ashrafian & Andersson 2006*a*). These different characteristics of the transport mechanism, in the outer layer, between boundary layer and channel flow may be related to different effects of surface roughness on Reynolds turbulent stresses in the outer layer.

Although the trends in the velocity triple products are similar for the smooth and rough walls, surface similarity in the outer layer, especially along the wall-normal direction, is not satisfied well when the products are normalized by the friction velocity and outer variables. Instead, we can define the third-order moments of velocity fluctuations M_i as

$$M^{ij} = \frac{\langle u^i v^j\rangle}{\langle u\rangle^i_{rms}\langle v\rangle^j_{rms}}, \quad i + j = 3, \quad i, j \geqslant 0.$$

Similarly to the Reynolds stress anisotropy tensor, the friction velocity is not used in this definition. Figure 16 shows good similarity of the third-order moments in the outer layer for smooth and rough walls. Thus, good surface similarity is observed for the Reynolds anisotropy tensors and third-order moments when they are normalized as outlined above, without using the friction velocity.

7. Conclusions

In the present study we sought to elucidate the effects of surface roughness on a TBL over a wall. To determine the basic information on the rough-wall TBL, we performed DNS of the TBLs over rough and smooth walls and compared the results with previous experimental data. Emphasis was placed on the interaction between the inner and outer layers induced by the surface roughness. The friction velocity was directly calculated from the total drag, which is the sum of the spatially averaged skin-frictional drag and form drag. In the rough-wall boundary layer, the friction velocity increased abruptly near the step change region and decreased slowly on moving downstream. The virtual origin was calculated as the centroid of the moment acting on the rod roughness. The virtual origin was placed at almost half of the roughness height from the wall and its streamwise variation was very small. Near

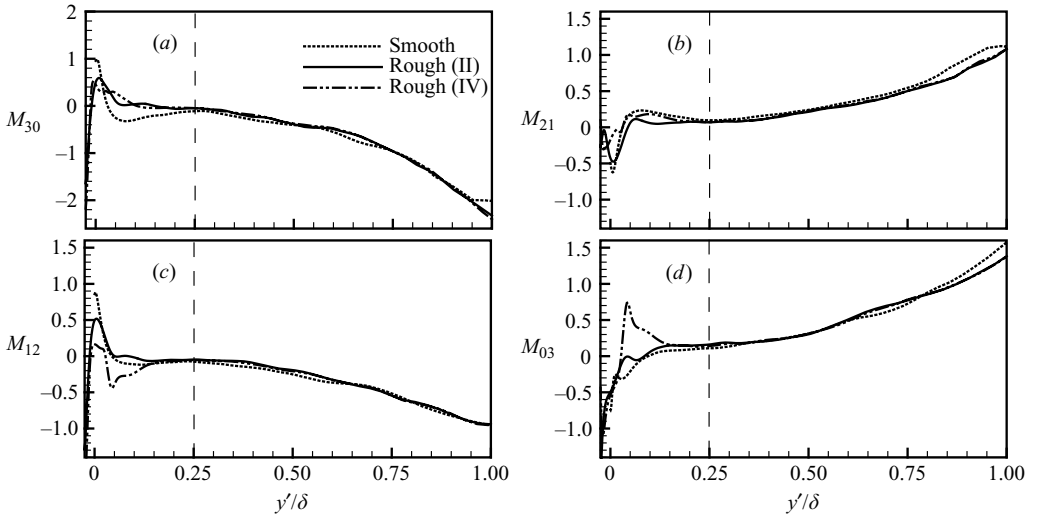

FIGURE 16. Third-order moments of velocity fluctuations: - - -, smooth; —, rod roughness at location II: – · · –, rod roughness at location.

the region where the surface changed from smooth to rough, the surface roughness significantly affected the turbulence statistics owing to blockage of the flow by the first rod. After the step change region, self-preservation of the Reynolds stresses was achieved after $x = 324\theta_{in}$. In the rough-wall simulations, the domain size along the streamwise direction was sufficiently long for the flow to reach a new equilibrium state above the rough wall. The roughness sublayer was estimated to have a thickness of about $y = 5k$. Above the roughness sublayer, the turbulence statistics collapsed well and were spatially homogeneous regardless their position relative to the rod roughness. The mean velocity-defect form showed very good surface similarity in the outer layer. However, the turbulent Reynolds stresses of the rough-wall flow differed from those of the smooth-wall flow not only inside the roughness sublayer, but also outside. By contrast, the Reynolds stress anisotropy tensor showed good surface similarity in the outer layer, indicating that no significant contribution is made to the ratio of each Reynolds stress component. Redistribution of the turbulent kinetic energy from $\langle u^{+2} \rangle$ to $\langle v^{+2} \rangle$ and $\langle w^{+2} \rangle$ is significantly affected by the surface roughness in the roughness sublayer, but not in the outer layer. In the region of the outer layer adjoining the roughness sublayer, the triple products of velocity fluctuations for the rough wall were stronger than those for the smooth wall. Increased sweep events were observed near the focal points of two recirculation regions in the cavity. Outside the cavity ($y > k$), the wall-normal velocity fluctuations were transported outward from the wall and ejection events were very strong above the leading edge. Large transport of $\langle u^{+2} \rangle$ and $\langle -u^{+}v^{+} \rangle$ were strongly related to these increased sweep and ejection events. In the outer layer, a loss of kinetic energy occurred, which was transported away from the wall. The transport mechanism of TBL in the outer layer was different from that of channel flow and may be related to different effects of roughness in the outer layer. The surface similarity, for velocity triple products was not shown when normalized by the friction velocity and outer variables. However, the third-order moments of velocity fluctuations, which do not require normalization by the friction velocity, showed a better surface similarity, similar to Reynolds anisotropy tensors. The present DNS study showed a lack of surface similarity between rough

and smooth walls, indicating the strong interaction between the inner and outer layers induced by the surface roughness. This was contrary to the previous findings of a DNS study of turbulent channel flow with the same two-dimensional rod-roughened wall. These findings indicate that the wall similarity criteria may be not universal to all flow types, and support the conjecture that surface roughness effects on the outer layer depends also on the outer boundary condition. It seems plausible that the lack of surface similarity is related to other factors, e.g. large roughness height, geometrical characteristics of rod roughness or low Reynolds number, etc. A DNS study with smaller roughness height and higher Reynolds number may be able to verify the wall similarity hypothesis more clearly, which will be a challenging undertaking.

Appreciation is extended to Professor P.-Å. Krogstad for his valuable discussion in the course of this study. This work was supported by the Basic Research Program (R01-2004-000-10521-0) of the Korea Science & Engineering Foundation and partially supported by the Grand Challenge Supercomputing Program of the Korea Institute of Science and Technology Information with Drs Lee and Ali as the technical support.

REFERENCES

Andreopoulos, J. & Bradshaw, P. 1981 Measurements of turbulence structure in the boundary layer on a rough surface. *Boundary-Layer Met.* **20**, 201–213.

Antonia, R. A. & Krogstad, P.-Å. 2001 Turbulence structure in boundary layers over different types of surface roughness. *Fluid Dyn. Res.* **28**, 139–157.

Antonia, R. A. & Luxton, R. E. 1971 The response of a turbulent boundary layer to a step change in surface roughness Part 1. Smooth to rough. *J. Fluid Mech.* **48**, 721–761.

Ashrafian, A., Andersson, H. I. & Manhart, M. 2004 DNS of turbulent flow in a rod-roughened channel. *Intl. J. Heat Fluid Flow* **25**, 373–383.

Ashrafian, A. & Andersson, H. I. 2006*a* The structure of turbulence in a rod-roughened channel. *Intl J. Heat Fluid Flow* **27**, 65–79.

Ashrafian, A. & Andersson, H. I. 2006*b* Roughness effects in turbulent channel flow. *Prog. Comput. Fluid Dyn.* **6**, 1–20.

Bakken, O. M. & Krogstad, P.-Å, Ashrafian, A. & Andersson, H. I. 2005 Reynolds number effects in the outer layer of the turbulent flow in a channel with rough walls. *Phys. Fluids* **17**, 065101.

Bandyopadhyay, P. R. & Watson, R. D. 1988 Structure of rough-wall boundary layers. *Phys. Fluids* **31**, 1877–1883.

Bhaganagar, K., Kim, J. & Coleman, G. 2004 Effect of roughness on wall-bounded turbulence. *Flow, Turbulence Combust.* **72**, 463–492.

Bisceglia, S., Smalley, R. J., Antonia, R. A. & Djenidi, L. 2001 Rough-wall turbulent boundary layers at relatively high Reynolds number. *Proc. 14th Australasian Fluid Mechanics Conference*, vol. 1, pp. 195–198.

Connelly, J. S., Schultz, M. P. & Flack, K. A. 2006 Velocity-defect scaling for turbulent boundary layers with a range of relative roughness. *Exps. Fluids* **40**, 188–195.

Djenidi, L., Elavarasan, R. & Antonia, R. A. 1999 The turbulent boundary layer over transverse square cavities. *J. Fluid Mech.* **395**, 271–294.

Flack, K. A., Schultz, M. P. & Shapiro, T. A. 2005 Experimental support for Townsend's Reynolds number similarity. *Phys. Fluids* **17,** 035102.

Grass, A. J., Stuart, R. J. & Mansor-Tehrani, M. 1993 Common vortical structure of turbulent flows over smooth and rough boundaries. *AIAA J.* **31**, 837–847.

Jackson, P. S. 1981 On the displacement height in the logarithmic profiles. *J. Fluid Mech.* **111**, 15–25.

Jimenez, J. 2004 Turbulent flows over rough walls. *Annu. Rev. Fluid Mech.* **36**, 173–196.

Keirsbulck, L., Labraga, L., Mazouz, A. & Tournier, C. 2002*a* Surface roughness effects on turbulent boundary layer structures. *Trans.* ASME: *J. Fluids Engng* **124**, 127–135.

Keirsbulck, L., Labraga, L., Mazouz, A. & Tournier, C. 2002*b* Influence of surface roughness on anisotropy boundary layer flow. *Exps. Fluids* **33**, 497–499.

Kim, J., Kim, D. & Choi, H. 2001 An immersed boundary finite-volume method for simulations of flow in complex geometries. *J. Comput. Phys.* **171**, 132–150.

Kim, K., Baek, S.-J. & Sung, H. J. 2002 An implicit velocity decoupling procedure for the incompressible Navier-Stokes equations. *Intl. J. Numer. Meth. Fluids* **38**, 125–138.

Krogstad, P.-Å., Antonia, R. A. & Browne, L. W. B. 1992 Comparison between rough- and smooth-wall turbulent boundary layers. *J. Fluid Mech.* **245**, 599–617.

Krogstad, P.-Å. & Antonia, R. A. 1994 Structure of turbulent boundary layers on smooth and rough walls. *J. Fluid Mech.* **277**, 1–21.

Krogstad, P.-Å. & Antonia, R. A. 1999 Surface roughness effects in turbulent boundary layers. *Exps. Fluids* **27**, 450–460.

Krogstad, P.-Å., Andersson, H. I., Bakken, O. M. & Ashrafian, A. 2005 An experimental and numerical study of channel flow with rough walls. *J. Fluid Mech.* **530**, 327–352.

Lee, C. 2002 Large-eddy simulation of rough-wall turbulent boundary layers. *AIAA J.* **40**, 2127–2130.

Leonardi, S., Orlandi, P., Smalley, R. J., Djenidi, L. & Antonia, R. A. 2003 Direct numerical simulations of turbulent channel flow with transverse square bars on one wall. *J. Fluid Mech.* **491**, 229–238.

Lund, T. S., Wu, X. & Squires, K. D. 1998 Generation of turbulent inflow data for spatially-developing boundary layer simulation. *J. Comput. Phys.* **140**, 233–258.

Mazouz, A., Labraga, L. & Tournier, C. 1998 Anisotropy invariants of Reynolds stress tensor in a duct flow and turbulent boundary layer. *Trans. ASME: J. Fluids Engng* **120**, 280–284.

Raupach, M. R., Antonia, R. A. & Rajagopalan, S. 1991 Rough-wall turbulent boundary layers. *Appl. Mech. Rev.* **44**, 1–25.

Sabot, J., Saleh, I. & Compte-Bellot, G. 1977 Effects of roughness on the intermittent maintenance of Reynolds shear stress in pipe flow. *Phys. Fluids* **20**, S150–S155.

Schultz, M. P. & Flack, K. A. 2003 Turbulent boundary layers over surfaces smoothed by sanding. *Trans. ASME: J. Fluids Engng* **125**, 863–870.

Schultz, M. P. & Flack, K. A. 2005 Outer layer similarity in fully rough turbulent boundary layers. *Exps. Fluids* **38**, 328–340.

Shafi, H. S. & Antonia, R. A. 1995 Anisotropy of the Reynolds stresses in a turbulent boundary layer on a rough wall. *Exps. Fluids* **18**, 213–215.

Smalley, R. J., Antonia, R. A. & Djenidi, L. 2001 Self-preservation of rough-wall turbulent boundary layers. *Eur. J. Mech.* B-*Fluids* **20**, 591–602.

Smalley, R. J., Leonardi, S., Antonia, R. A., Djenidi, L. & Orlandi, P. 2002 Reynolds stress anisotropy of turbulent rough wall layers. *Exps. Fluids* **33**, 32–37.

Spalart, P. R. 1988 Direct simulation of a turbulent boundary layer up to $Re_\theta = 1410$. *J. Fluid Mech.* **187**, 61–98.

Townsend, A. A. 1976 *The Structure of Turbulent Shear Flow*. Cambridge University Press.